Eur. Phys. J. Plus (2021) 136:315
https://doi.org/10.1140/epjp/s13360-021-01294-2

THE EUROPEAN PHYSICAL JOURNAL PLUS

Regular Article

Dynamics of multiple solutions of Darcy–Forchheimer saturated flow of Cross nanofluid by a vertical thin needle point

Pei-Ying Xiong[1], Aamir Hamid[2], Yu-Ming Chu[3,4,a], M. Ijaz Khan[5], R. J. Punith Gowda[6], R. Naveen Kumar[6], B. C. Prasannakumara[6], Sumaira Qayyum[2]

[1] College of Science, Hunan City University, Yiyang 413000, People's Republic of China
[2] Department of Mathematics, Quaid-i-Azam University, Islamabad 45320, Pakistan
[3] Department of Mathematics, Huzhou University, Huzhou 313000, People's Republic of China
[4] Hunan Provincial Key Laboratory of Mathematical Modeling and Analysis in Engineering, Changsha University of Science and Technology, Changsha 410114, People's Republic of China
[5] Department of Mathematics and Statistics, Riphah International University I-14, Islamabad 44000, Pakistan
[6] Davangere University, Davangere, Karnataka, India

Received: 13 February 2021 / Accepted: 3 March 2021

Abstract Nanofluids have exposed a significant promise in the thermal development of several industrial systems, and at the same time, the flow via needle has major applications in modern construction systems including microstructure electric gadgets and microscale cooling gadgets for thermal migration applications. According to these applications, the current investigation concentrates to deliberate on 2D steady, laminar and incompressible flow of magneto-Cross nanofluid towards the region of moving thin needle in the occurrence of Darcy–Forchheimer porous medium, Ohmic and viscous dissipation with chemical reaction and mixed convection. The new dimensionless similarity variables are introduced to convert the nonlinear expressions governing the flow and transfer of heat. The change in velocity, thermal and concentration profiles for various non-dimensional parameters is deliberated briefly and illustrated with the help of suitable plots. Further, analysis of skin friction and rate of heat transfer is done through graphs. The results obtained are validated by existing works and are found to have a good agreement. The result outcome reveals that advanced values of magnetic parameter and Weissenberg number slowdown the fluid velocity motion. Also, upshot in Brownian motion and thermophoresis parameters improves the thermal profile.

List of symbols

u, v	Velocity components
x, r	Axial and radial coordinates
θ	Dimensionless temperature
T	Fluid temperature
C	Fluid concentration

[a] e-mail: chuyuming@zjhu.edu.cn (corresponding author)

Published online: 12 March 2021

T_w	Surface temperature
C_∞	Ambient nanoparticle volume fraction
C_w	Surface volume fraction
ρ	Fluid density
$(\rho c)_p$	Effective heat capacity of a nanoparticle
T_∞	Ambient temperature
c_p	Specific heat
k	Thermal conductivity
B_0	Magnetic parameter
a	Needle thickness size
U_∞	Free stream velocity
ψ	Stream function
α	Thermal diffusivity
Le	Lewis number
τ	Parameter defined by the ratio $\frac{(\rho c)_p}{(\rho c)_f}$
R	Radiation parameter
f	Dimensionless stream function
Pr	Prandtl number
μ	Generalized Newtonian viscosity
Re	Local Reynolds number
n	Power law index
η	Dimensionless similarity variable
$(\rho c)_f$	Heat capacity of the base fluid
Ec	Eckert number
μ_0	Zero shear viscosity
μ_∞	Infinite shear viscosity
ϕ	Dimensionless concentration
ν	Kinematic viscosity
Γ	Relaxation time
τ_w	Surface shear stress
M	Magnetic parameter
We	Weissenberg number
$\dot{\gamma}$	Magnitude of deformation rate
Nu	Local Nusselt number
C_f	Skin friction coefficient
U_w	Stretching velocity
Nt	Thermophoresis diffusion
Nb	Brownian motion

1 Introduction

Flow and temperature analysis in a moving thin needle has been evaluated by many researchers with several flow problems, because of the importance of various applications in machinery and industries like microscale cooling system, heat transfer apparatuses, a hot wire anemometer and microstructure electric implements that promote high performance with durability and much more. The name of the tiny needle is seen as a change in the direction of its axis depending on the size. Chen and smith [1] analytically scrutinized the steady

laminar forced convective transfer of heat in non-uniform incompressible flows through non-isothermal tinny needles. Ishak et al. [2] used finite- difference method to illustrate the flow on a poignant isothermal tinny needle analogous to a stirring flow. The encouragement of nonlinear thermal radiation effect on Casson nanoliquid flow along tinny needle on taking account of double diffusion effects was illustrated by Souayeh et al. [3]. Recently, the effect of variable buoyancy force, viscid dissipation and Ohmic heating on the nanoliquids flow through poignant slim needle was scrutinized by Nayak et al. [4]. Chu et al. [5] inspected the impact of homogenous–heterogeneous reactions and internal diffusion of particle on the thin needle surface on taking account of radiative heat flux.

To improve the utilization of fossil fuels and to decrease environmental issues, present day nanotechnology has proposed different assets work more closely with the interaction of nanoparticles. Due to the high thermal performance, nanoparticles are gaining valuable scientific value in the fields of engineering, chemical and mechanical industries. Nanofluid is a combination of nanoparticle with a carrier liquid, and it was first proposed by Choi [6] in 1995. He evidenced that the thermal performance of a small amount of active fluid like water is improved by the appropriate use of these nanoparticles. This humorous concept is widely accepted by many researchers to test heat transfer in various flow conditions. Khan et al. [7] scrutinized impact of energy of activation in MHD flow past an enlarging surface on taking account of mixed convection and chemical reaction. Azam et al. [8] scrutinized the influence of heat origination/sink in unsteady Cross nanoliquid through an escalating /constricting cylinder. Hayat et al. [9] utilized Cross fluid model to investigate MHD flow of Newtonian liquid past a stretchy surface. The various features in minimization of entropy production for Cross nanofluid flow towards a stretchy surface with Lorentz's forces were scrutinized by Ali et al. [10].

Fluid flow along with Darcy–Forchheimer porous medium has a wide range of applications for distribution and critical importance to medicine and modern environmental structures. The classic Darcy model was built on a non-Darcian-based version that was a limited version of this method when referring to the applications and procedures mentioned above. This model was explained by Darcy [11]. It was a total limited porosity type and velocity field for higher velocities. Forchheimer [12] updated this model which calculates the name of the square in proportion to the solidarity. Later, this medium was named as Darcy–Forchheimer medium by Muskat [13]. Recently, Khan et al. [14] scrutinized analysis of entropy production and mixed convective flow of viscous fluid past a stretchable surface of disk on taking account of convective and second-order velocity slip constraints in a Darcy–Forchheimer permeable medium. Hayat et al. [15] scrutinized the impact of mixed convection and heat source/sink on Darcy–Forchheimer flow of viscous liquid induced by a nonlinear inclined stretching surface. Reddy et al. [16] scrutinized the consequence of viscid dissipation on Darcy–Forchheimer flow of a viscoelastic liquid over a continuous poignant slim needle.

The consequence of Ohmic heating with a magnetic effect plays a key role in nuclear engineering. Joule or Ohmic heating is a process in which electrical energy flows into any object and, at the same time, generates heat. Many researchers studied the boundary layer flow problems with Joule heating on different geometrical shapes. Shashikumar et al. [17] scrutinized the two-dimensional Brinkman–Forchheimer flow in a microchannel on taking account of multiple slips viscid dissipation and Ohmic heating. The impact of Ohmic heating and melting effect on magnetohydrodynamic flow of viscous liquid through a stretchy plate was deliberated by Hayat et al. [18]. Radhika et al. [19] analyzed the encouragement of magnetic effect on dusty hybrid nanoliquid flow. Ijaz et al. [20] deliberated the impact of activation energy on flow of a Sisko nanoliquid due to a rotating disk with stretching on taking account of inhomogeneous heat origination/sink and radiation effect. Mixed convective flow through

fluid filled geometries has extensive range of applications in several engineering systems like solar collectors, solar ponds, heat exchangers and food industry. Several researchers studied mixed convective flow of different fluids through diverse geometries [21–25]. Many notable works have been done by several researchers in the field of multiple solutions for Newtonian nanofluid flow and transfer of heat [26–30].

Encouraged by above works, our main aim of current investigation is to examine the steady, laminar and incompressible flow of magneto-Cross nanofluid towards the region of moving thin needle placed in Darcy–Forchheimer permeable medium. The influence of mixed convection, Ohmic and viscous dissipation with chemical reaction is invoked. The assumed flow is represented in terms of PDEs and are converted to ODEs by opting suitable similarity variables. We have obtained excellent results which agree with previously published works.

2 Problem formulation

Let us assume the steady, laminar and incompressible flow of magneto-Cross nanofluid towards the region of moving thin needle in the occurrence of Darcy–Forchheimer porous medium. The influence of mixed convection, Ohmic and viscous dissipation with chemical reaction is invoked. The needle is continuously moving with uniform velocity U_w, in the similar and reverse direction with the fluid flow of a constant velocity U_∞. The magnetic field of strength $B = B_0$ is imposed radially. Nonlinear radiation and heat source/sink effects are considered in energy equation. It is assumed that temperature and concentration of the thin needle surface are T_w and C_w, respectively. Further, the temperature and concentration of free stream region (T_∞, C_∞) are considered to be constant such that $T_w > T_\infty$ and $C_w > C_\infty$. The geometry of the modeled problem is described in Fig. 1 with (u, v) denoting (x, r) components of velocity and $R(x) = \left(\frac{\nu a x}{U}\right)^{1/2}$ depicts the needle radius.

In line with these assumptions and using Buongiorno's nanofluid model, the continuity, momentum, energy and concentration equations of the unsteady Cross fluid flow past a vertically moving thin needle yield the form [5]:

$$\frac{\partial}{\partial x}(ru) + \frac{\partial}{\partial r}(rv) = 0, \tag{1}$$

$$u\frac{\partial u}{\partial x} + v\frac{\partial u}{\partial r} = \nu\left(\frac{\partial}{\partial r} + \frac{1}{r}\right)\left[\left(\frac{\partial u}{\partial r}\right)\left\{1 + \left(\Gamma\left|\frac{\partial u}{\partial r}\right|\right)^n\right\}^{-1}\right] - \frac{\sigma B_0^2 u}{\rho} - \nu\left(\frac{\phi_1}{K^*}\right)u - Fu^2 + \frac{1}{\rho_f}\left[(1 - C_\infty)\rho_{f_\infty}\beta_T(T - T_\infty) - \left(\rho_p - \rho_{f_\infty}\right)(C - C_\infty)\right]g, \tag{2}$$

$$u\frac{\partial T}{\partial x} + v\frac{\partial T}{\partial r} = \frac{k}{\rho c_p}\frac{1}{r}\frac{\partial}{\partial r}\left[\left(1 + \frac{16\sigma_s}{3k_e k_f}T_\infty^3\right)\left(r\frac{\partial T}{\partial r}\right)\right] + \frac{\nu}{c_p}\left\{1 + \left(\Gamma\left|\frac{\partial u}{\partial r}\right|\right)^n\right\}^{-1}\left(\frac{\partial u}{\partial r}\right)^2 + \frac{\sigma B_0^2 u^2}{\rho c_p} + \tau\left[\frac{D_T}{T_\infty}\left(\frac{\partial T}{\partial r}\right)^2 + D_B\frac{\partial T}{\partial r}\frac{\partial C}{\partial r}\right] + \frac{Q_0}{\rho c_p}(T - T_\infty), \tag{3}$$

$$u\frac{\partial C}{\partial x} + v\frac{\partial C}{\partial r} = D_B\frac{\partial^2 C}{\partial r^2} + \frac{D_T}{T_\infty}\frac{\partial^2 T}{\partial r^2} - k^*(C - C_\infty), \tag{4}$$

with boundary conditions

$$u = U_w,\ v = 0,\ T = T_w,\ D_B\frac{\partial C}{\partial r} + \frac{D_T}{T_\infty}\frac{\partial T}{\partial r} \text{ at } r = R(x),$$
$$u \to U_\infty,\ T \to T_\infty,\ C \to C_\infty,\ \text{as } r \to \infty. \tag{5}$$

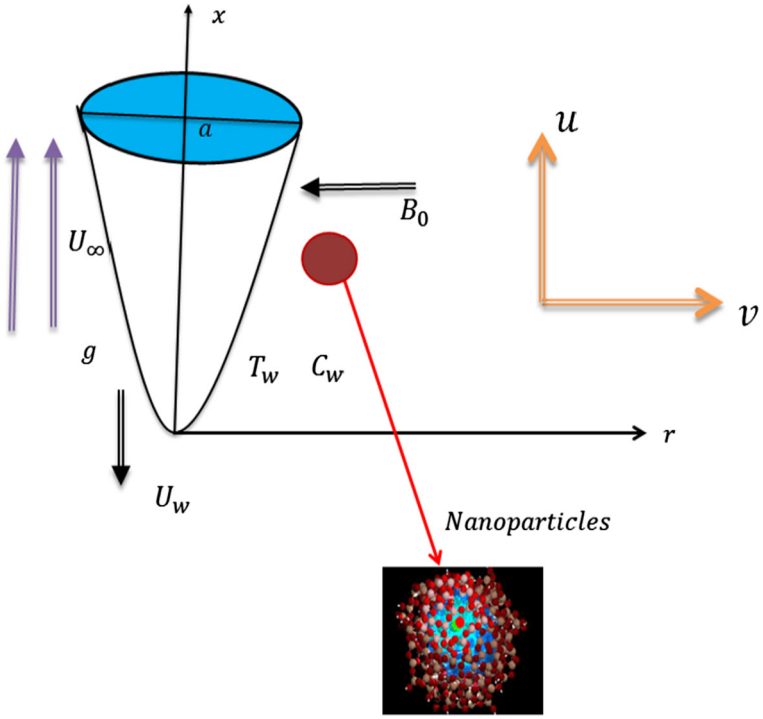

Fig. 1 Physical model and coordinate system

We introduce the similarity transformations; $\eta = \frac{Ur^2}{x\nu}$, $\psi = \nu x f(\eta)$, $\theta(\eta) = \frac{T-T_w}{T_w-T_\infty}$ and $\phi(\eta) = \frac{C-C_\infty}{C_\infty}$. Here, ψ is the stream function that satisfies the continuity equation with $u = \frac{1}{r}\frac{\partial \psi}{\partial r}$ and $v = -\frac{1}{r}\frac{\partial \psi}{\partial x}$ and then the governing PDEs finally reduce to

$$\mathrm{Re}\left[1+(1-n)(4\mathrm{We}f'')^n\right]f''' + \frac{1}{2}\left[1+(4\mathrm{We}f'')^n\right]^2 + ff'' - (M+\lambda_1)f' - Frf'^2 + \frac{\lambda\theta}{4} - \frac{\mathrm{Nr}\phi}{4} = 0, \tag{6}$$

$$\frac{1}{\mathrm{Pr}}\left[1+R(1+(\theta_w-1)\theta)^3\left(\eta\theta'\right)\right]' + f\theta' + \left[\frac{\left(f''\right)^2}{[1+(4\mathrm{We}f'')^n]}\right]4\mathrm{Ec}\eta + \mathrm{ME}cf'^2 + \frac{1}{2}Q\theta + 2\eta\left(\mathrm{Nt}\theta'^2 + \mathrm{Nb}\theta'\phi'\right) = 0, \tag{7}$$

$$2\eta\phi'' + 2\phi' + \mathrm{Le}\,\mathrm{Pr}\,f\phi' + 2\eta\frac{\mathrm{Nt}}{\mathrm{Nb}}\theta'' + 2\frac{\mathrm{Nt}}{\mathrm{Nb}}\theta' - \frac{1}{2}\mathrm{Le}\,\mathrm{Pr}\,K\phi = 0. \tag{8}$$

The boundary condition becomes

$$f(a) = \frac{\varepsilon}{2}a,\ f'(a) = \frac{\varepsilon}{2},\ \theta(a) = 1,\ \mathrm{Nt}\theta'(a) + \mathrm{Nb}\phi'(a),$$
$$f'(\eta) \to \frac{1-\varepsilon}{2}, \theta(\eta) \to 0, \phi(\eta) \to 0 \text{ as } \eta \to \infty. \tag{9}$$

Besides, assume $\eta = a$ to show the thickness or size of the needle.

Here, We, M, λ_1, Fr, λ,ϕ_1, $k*$, Nr, Pr, R, Ec, Q, Nt, Nb, Le, K, Re and ε represent the Weissenberg number, magnetic parameter, porosity parameter, non-uniform inertia coefficient, porosity of porous medium, permeability of porous space, mixed convection parameter,

Table 1 Comparison of $f''(a)$ for some reduced cases when $\varepsilon = M = \mathrm{Nr} = \lambda_1 = \lambda = \mathrm{Fr} = 0$ and $\mathrm{We} \to 0$

A	0.1	0.01	0.001
Chen and Smith [1]	1.28881	8.49244	62.16372
Ishak et al. [2]	1.2888	8.4924	62.1637
Souayeh et al. [3]	1.288801	8.492412	62.16371
Present study	1.28880151	8.49241223	62.1637124

buoyancy ratio parameter, Prandtl number, radiation parameter, Eckert number, Heat generation parameter, Brownian motion parameter, thermophoresis parameter, Lewis number, chemical reaction parameter and velocity ratio parameter between the needle and free stream surface with $U = U_w + U_\infty \neq 0$.

These dimensionless parameters are stated below:

$\mathrm{We} = \frac{U_w \mathrm{Re}}{U}$, $M = \frac{\sigma B_0^2 x}{2\rho U}$, $\lambda_1 = \frac{\nu \phi_1}{c k*}$, $\lambda = \frac{\mathrm{Gr}_x}{\mathrm{Re}^2}$ (where $\mathrm{Gr}_x = \frac{(1-C_\infty)(T-T_\infty) g \beta_T x^3}{\nu^2}$ and $\mathrm{Re} = \frac{Ux}{\nu}$,$\mathrm{Nr} = \frac{(\rho_p - \rho_{f\infty}) C_\infty g x}{U^2 \rho_f}$,

$\mathrm{Pr} = \frac{\rho c_p \nu}{k}$, $R = \frac{16\sigma_s T_\infty^3}{3k_e k_f}$, $\mathrm{Ec} = \frac{2U^2}{c_p (T_w - T_\infty)}$, $Q = \frac{Q_0 x}{\rho c_{pU}}$, $\mathrm{Nt} = \frac{\tau D_T (T_w - T_\infty)}{\nu T_\infty}$, $\mathrm{Nb} = \frac{\tau D_B C_\infty}{\nu}$, $\mathrm{Le} = \frac{\alpha}{D_B}$, $K = \frac{K_0 x}{U}$, and $\varepsilon = \frac{U_w}{U}$.

It is important to remember that the value of velocity ratio parameter $\varepsilon (0 < \varepsilon < 1)$ is critical and specifies the enhancement of the liquid and needle in distinct directions.

2.1 Quantities of physical interest

The quantities of physical interest are skin friction coefficient C_f and Nusselt number Nu, which are stated as

$$\mathrm{Re}^{1/2} C_f = \frac{2\mu}{\rho U_w^2} \left\{ 1 + \left(\Gamma \left| \frac{\partial u}{\partial r} \right| \right)^n \right\}^{-1} \left(\frac{\partial u}{\partial r} \right)_{r=R} = 8a^{1/2} \left[\frac{f''(a)}{\left[1 + \mathrm{We} |f''(a)|^n \right]} \right],$$

$$Re^{-1/2} \mathrm{Nu} = -\frac{x}{(T_w - T_\infty)} \left(\frac{\partial T}{\partial r} \right)_{r=R} + q_r = -2a^{1/2} \left(1 + R(1 + (\theta_w - 1)\theta(a))^3 \right) \theta'(a). \tag{10}$$

2.2 Numerical scheme and validation

The accompanying differential equation system (6–8) with boundary conditions (9) is numerically solved using the effective numerical method known as the Runge–Kutta–Fehlberg (RKF-45) shooting scheme method. The ruling equations are first decomposed into a system of first-order differential equations, and with the aid of MATLAB software, the shooting method is used for step-by-step integration. The dual branch of solutions is accomplished in this approach by allowing separate initial guesses to be made. Here, the stepsize $\Delta\eta = 0.001$ is chosen to get the desired convergence criterion of 10^{-5} in nearly all cases. Table 1 demonstrates the high precision of the Chen and Smith [1], Ishak et al. [2] and Souayeh et al. [3] results.

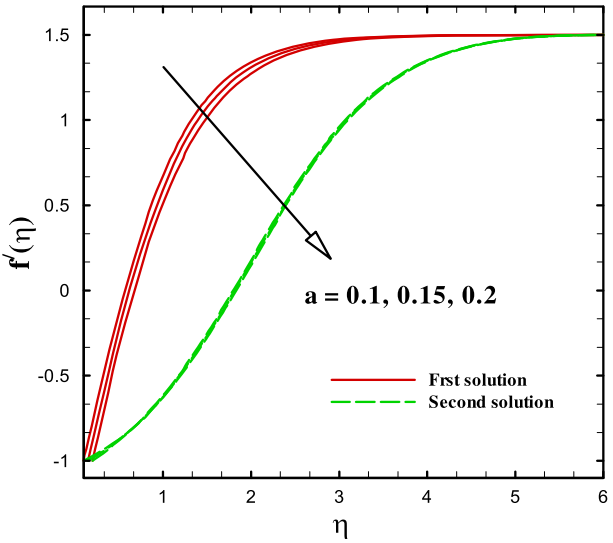

Fig. 2 $f'(\eta)$ for several values of a

3 Results and discussion

This section is dedicated to visualizing the physical insight of graphical illustration for 2D steady, laminar and incompressible flow of magneto-Cross nanofluid towards the region of moving thin needle in the existence of mixed convection, Darcy–Forchheimer permeable medium, Ohmic and viscous dissipation with chemical reaction. A numerical scheme is applied to provide a clear understanding and are sufficient to depict the behavior of flow profiles, which are strategized and deliberated with the assistance of graphs. A magnificent agreement between the outcomes is found for the extraordinary instance of the current issue. Here, we are anxious with giving the severity of the non-dimensional velocity and thermal fields as well as friction factor and rate of heat transfer in contrast to any difference in the physical parameters involved, namely velocity ratio parameter between the needle and free stream surface (ε). Weissenberg number We, porosity parameter λ_1, magnetic parameter M, mixed convection parameter λ, non-uniform inertia coefficient Fr buoyancy ratio parameter Nr, radiation parameter R, Prandtl number Pr, heat generation parameter Q, thermophoresis parameter Nt, Lewis number Le, Brownian motion parameter Nb, Eckert number Ec and chemical reaction parameter K. Similarity equalities (6–8) with boundary constraints (9) are highly nonlinear coupled ODEs. This complex system is tough to solve with the standard analytic methods, so we use the RKF-45 numerical method by adopting shooting process. The choice of the first guess and the size of the boundary layer η_∞ depends on the parameters values which are used to find the essential solutions. Also, the developed convergent series solutions are also numerically justified in Table 1. The study is carried out by considering two different solutions throughout the flow.

3.1 Effect of several parameters on velocity profile

Figures 2, 3, 4, 5, 6, 7, 8, 9, 10 and 11 display the change in velocity gradient for several values of a, M,We, λ, Ec, Nr, Q, Re, λ_1, Fr subjected to velocity gradient $f'(\eta)$. Figure 2

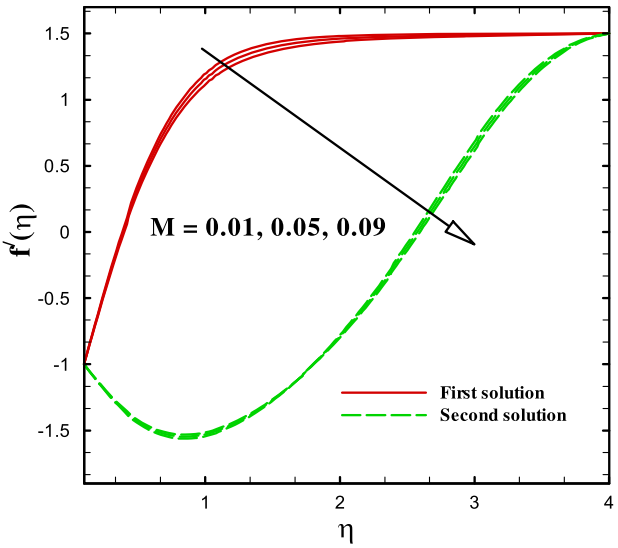

Fig. 3 $f'(\eta)$ for several values of M

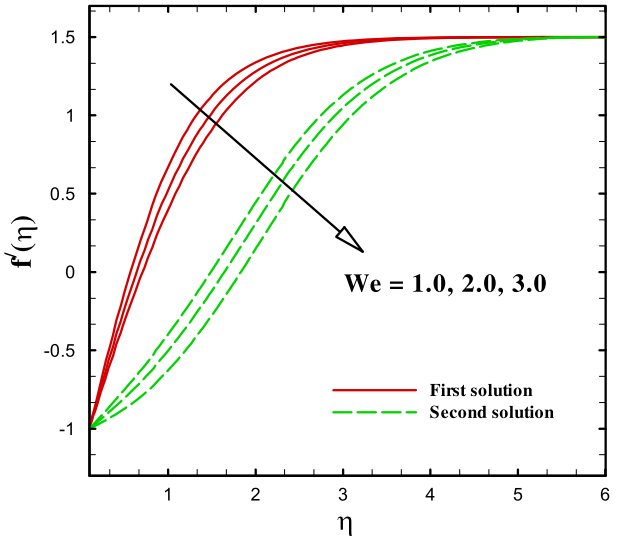

Fig. 4 $f'(\eta)$ for several values of We

encloses the behavior of reports on velocity gradient for upward values of a. The rising values of a decline the velocity profile for both the solutions as displayed in figure. Physically, with the increasing size of the needle, the surface of the thin needle when it comes in contact with the liquid particles grows, which works internally and improves drag force which is why the velocity decreases. In addition, the thickness of the velocity boundary layer upsurges with increasing needle stiffness. Figure 3 highlights the performance of magnetic parameter subjected to velocity gradient. Advanced values of induced magnetic field slowdown the fluid velocity motion and thickness of its boundary layer associated with it. Graph evidently

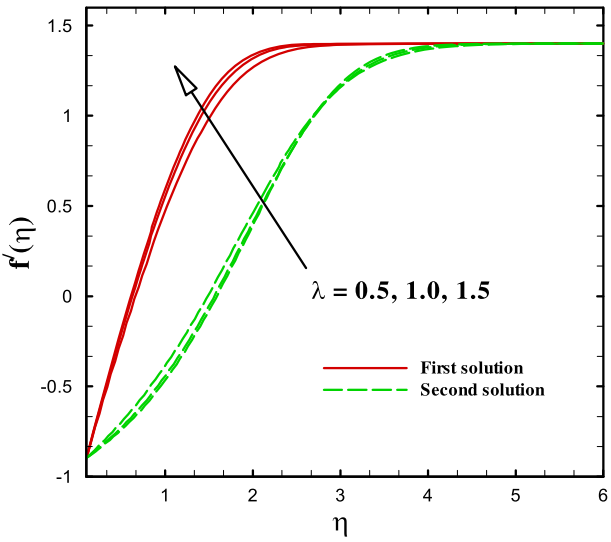

Fig. 5 $f'(\eta)$ for several values of λ

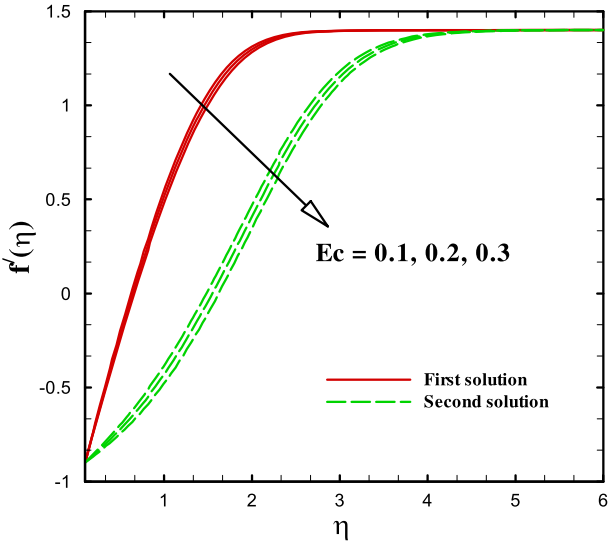

Fig. 6 $f'(\eta)$ for several values of Ec

reveals that the velocity of the second solution shows greater variation for higher values of magnetic parameter when compared to first solution. Here, more struggle is created to the fluid motion by Lorentz force, because the velocity profile declines. Figure 4 plots the aspects of velocity profile for shoot-up values of We. The figure exposes that rise in We declines the fluid velocity. Physically, Weissenberg number We is the ratio of relaxation time of the liquid and an exact process time. It upsurges the fluid thickness due to which the distribution of velocity diminutions. Also, it is observed in all the above cases that the second solution slowdowns faster and shows greater variations when compared to the first solution.

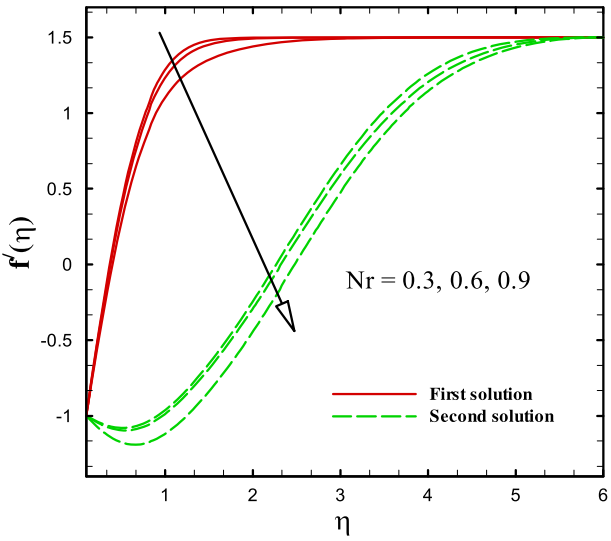

Fig. 7 $f'(\eta)$ for several values of Nr

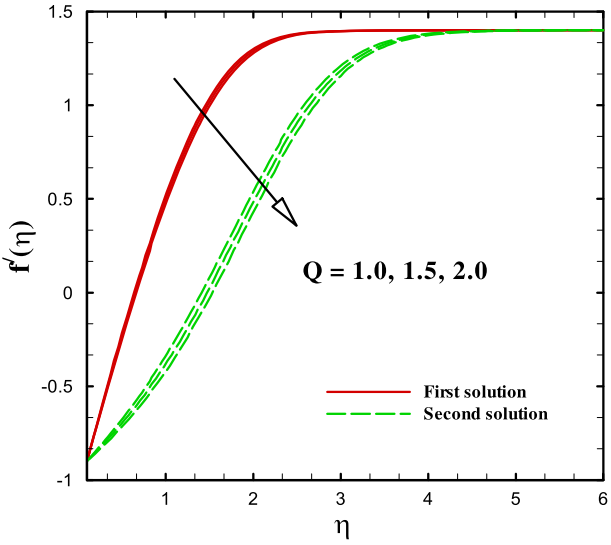

Fig. 8 $f'(\eta)$ for several values of Q

The sway of pattern for several values of λ subjected to velocity gradient is drafted in Fig. 5. Increasing values of λ incline the velocity of the fluid motion and thickness of its boundary layer associated with it. One can notice from the figure that the velocity of the fluid motion inclines faster in first solution when compared to second solution. Figure 6 illustrates the sway of pattern of $f'(\eta)$ for several values of Ec. One can see from figure that higher values of Ec decline the fluid velocity. Figure 7 depicts the sway of Nr on $f'(\eta)$. Results disclose that the rising values of Nr decrease the velocity of the fluid motion. Also, in these two conditions one can notice that the velocity of the fluid motion declines faster in second solution when

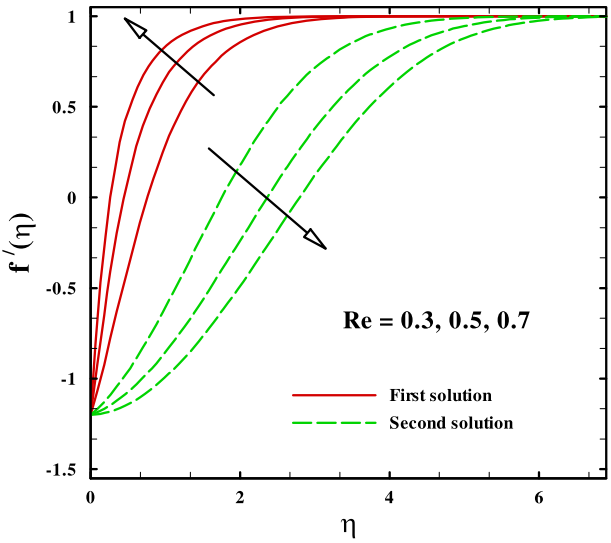

Fig. 9 $f'(\eta)$ for several values of Re

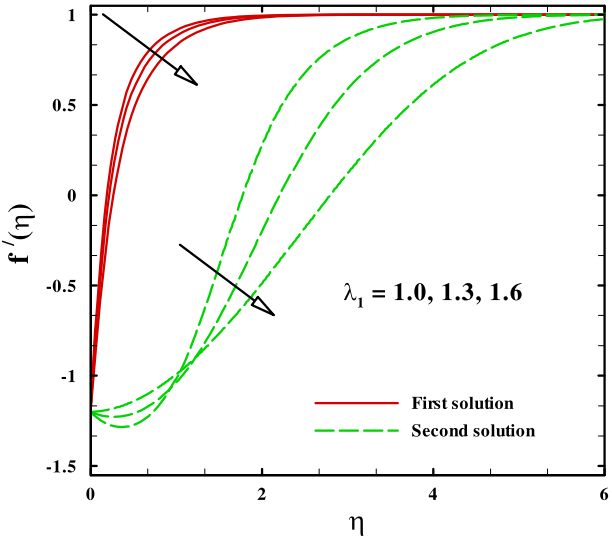

Fig. 10 $f'(\eta)$ for several values of λ_1

compared to first solution. Figure 8 illustrates the change of distribution in velocity profile for numerous values of Q. Inclining values of Q decline the velocity profile as depicted in Fig. 8. Figures 9, 10 and 11 establish the sway of pattern for velocity profile for Re, λ_1 and Fr, respectively. The absorbency factor becomes feebler compared to the increasing porosity parameter corresponding to low velocity gradients. Further, it is observed that velocity profile declines faster in second solution.

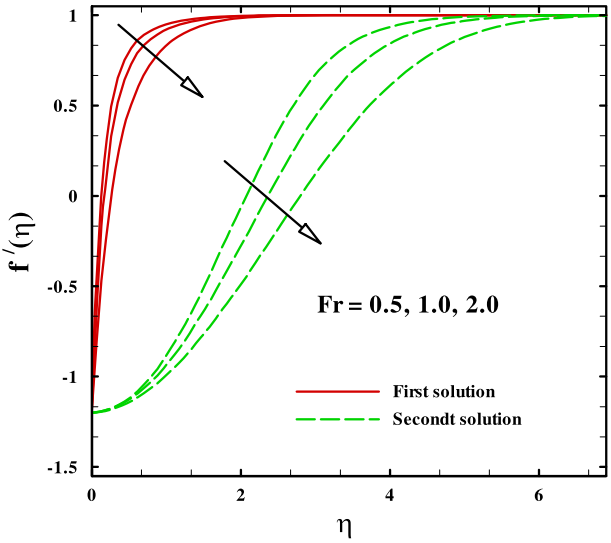

Fig. 11 $f'(\eta)$ for several values of Fr

3.1.1 Effect of numerous parameters on coefficient of skin friction

The influence of several dimensionless parameters on skin friction is portrayed in Figs. 12, 13 and 14. Variation of $\mathrm{Re}^{1/2}C_f$ with the influence of different values of We versus ε is depicted in Fig. 12. One can detect from figure that rise in values of a enhances the friction factor. Further, it is detected that skin friction improves in both cases for rise in values of a. Sway of M on $\mathrm{Re}^{1/2}C_f$ versus ε is portrayed in Fig. 13. The heightening of M declines the friction factor as depicted in figure. Here, $\mathrm{Re}^{1/2}C_f$ shows declining behavior in both solutions for rising values of M. Figure 14 demonstrates the influence of We on $\mathrm{Re}^{1/2}C_f$ versus ε. It is noticed from figures that upshot in values of We declines the $\mathrm{Re}^{1/2}C_f$ and $\mathrm{Re}^{1/2}C_f$ shows declining behavior for both cases. Here, we notice that ε acts as an increasing function of $\mathrm{Re}^{1/2}C_f$ as displayed in Figs. 12, 13 and 14.

3.1.2 Effect of numerous parameters on thermal profile

Figures 15, 16, 17, 18, 19 and 20 enclose the behavior of reports on temperature profile for various parameters for two different fluid solutions. Figure 15 captures the sway pattern of temperature gradient for numerous values of R. Upsurge in R declines the thermal profile as revealed in figure. Also, it is faster in first solution. Physically, radiation is considered to be a process of energy transfer which extracts energy by moving particles, which improves the thermal conductivity of moving liquid. Figure 16 shows the sway of Fr which realizes the change in flow and thermal gradients. A downfall of temperature appears as diminution of boundary layer thickness for diverse values of Fr that opposes the fluid motion and reduces the thermal profile. Also, one can notice that the thermal gradient declines faster in second solution when compared to first solution. Figure 17 plots the aspects of $\theta(\eta)$ for several values of θ_w. This plot shows that the rise in values of θ_w inclines the thermal profile. Figures 18, 19 describe the sway of pattern subjected to temperature profile for various values of Nb and Nt respectively. Increasing values of these parameters incline the temperature profile. This

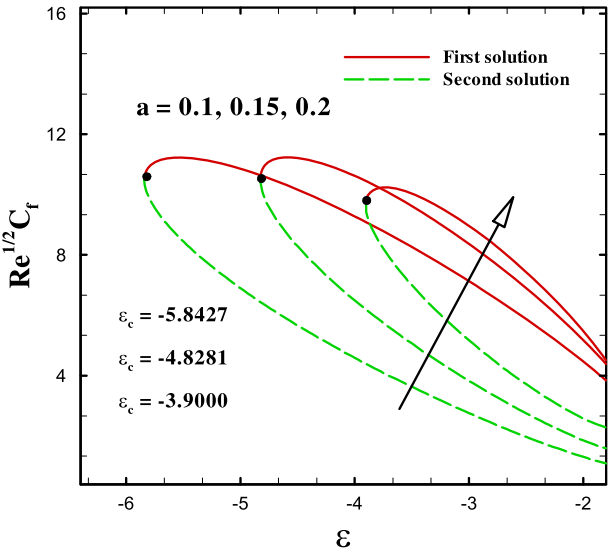

Fig. 12 Variation of $\mathrm{Re}^{1/2}C_f$ with ε for different values of a

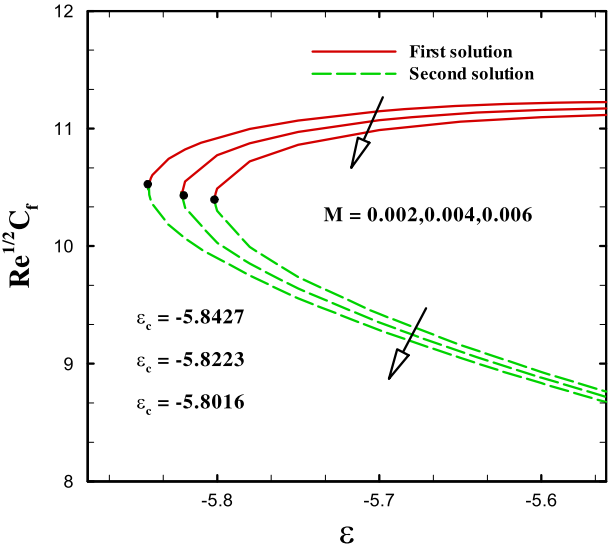

Fig. 13 Variation of $\mathrm{Re}^{1/2}C_f$ with ε for different values of M

is because the increase in the Nt indicates a characteristic that is directly opposes the flow of fluid to the appropriate flow zone. It is described as a measure of thermophoretic distribution due to the gradient of heat in the momentum diffusion on the nanofluid. The large Nt exhibits significant thermophoretic power. This involves the nanoparticles near the hot plate being pushed into the surrounding liquid. As a result, the speed of the liquid decreases near the surface of the moving slim needle and obviously inclines the thermal gradient. Also, it is observed that the thermal gradient inclines faster in second solution when compared to first

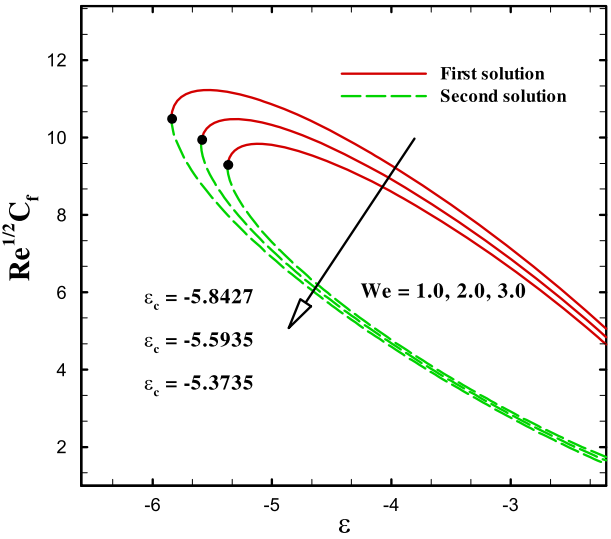

Fig. 14 Variation of $\mathrm{Re}^{1/2}C_f$ with ε for different values of We

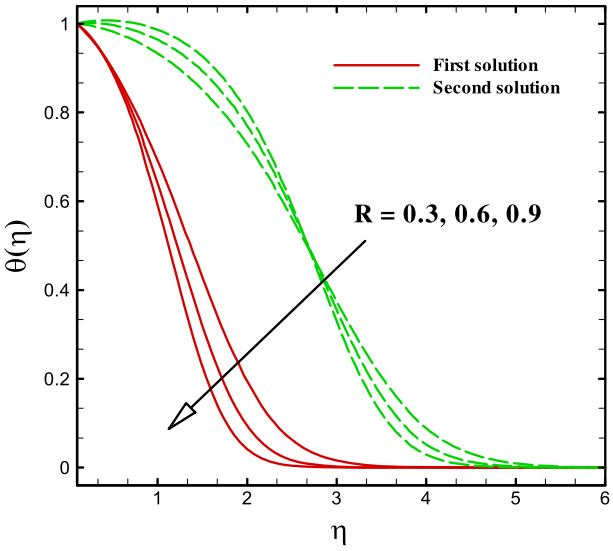

Fig. 15 $\theta(\eta)$ for several values of R

solution. Figure 20 conveys the representation of the liquid temperature in response to the Prandtl number. It is hypothesized that the fluid of the high Pr values with low thermal conductivity reduces the rate of heat transfer to the surface of the moving thin needle. Also, this graph demonstrates that the thermal gradient decays faster in first solution when compared to second solution.

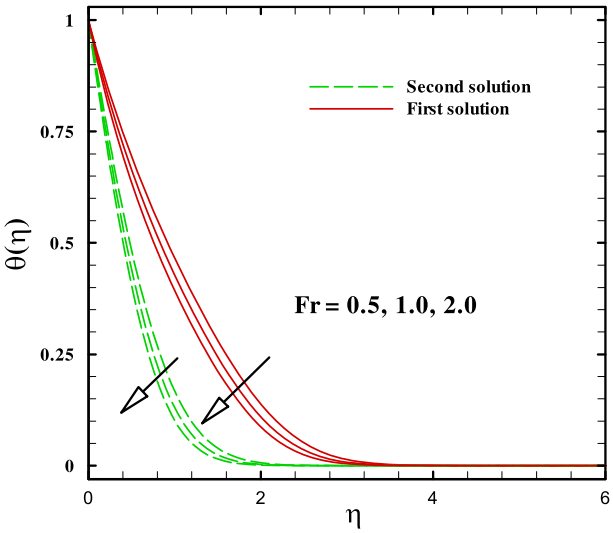

Fig. 16 $\theta(\eta)$ for several values of Fr

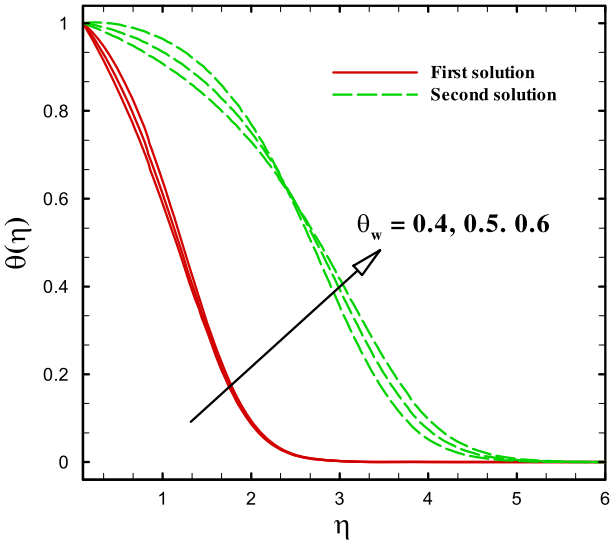

Fig. 17 $\theta(\eta)$ for several values of θ_w

3.1.3 Influence of numerous parameters on Nusselt number

The change in $\mathrm{Re}^{-1/2}Nu$ with ε for diverse values of a is displayed in Figs. 21, 22. The impact of a on rate of heat transfer is displayed in Fig. 21. Here, we discussed multiple solutions of heat transfer rate for diverse values of ε_c ($= -3.905, -4.8283, -5.8427$). One can observe from figure that Nusselt number shows declining behavior for shoot-up values of a in both the solution when ε_c ($= -3.905, -4.8283$) and it shows opposite behavior in both the solutions when $\varepsilon_c (= -5.8427)$. Figure 22 displays the variation in rate of heat

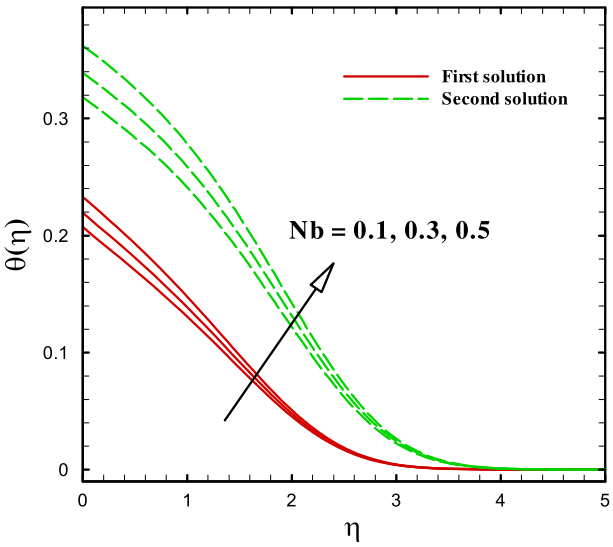

Fig. 18 $\theta(\eta)$ for several values of Nb

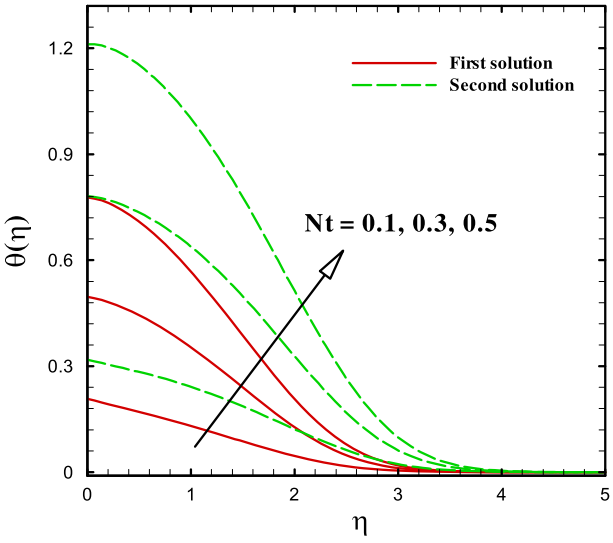

Fig. 19 $\theta(\eta)$ for several values of Nt

transfer for diverse values of R versus ε. It is observed from figure that a rise in values of a with $\varepsilon_c(= -5.8188, -5.8427, -5.9070)$ enhances the heat transfer rate in both the solutions and the rate of increase in Nusselt number is high in second solution when compared to first solution.

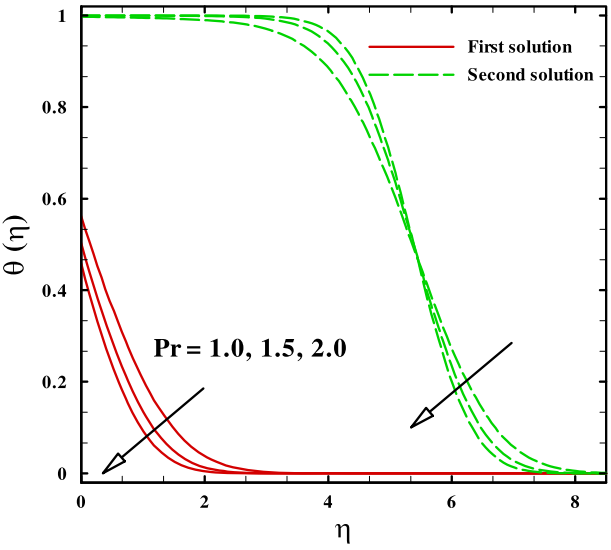

Fig. 20 $\theta(\eta)$ for several values of Pr

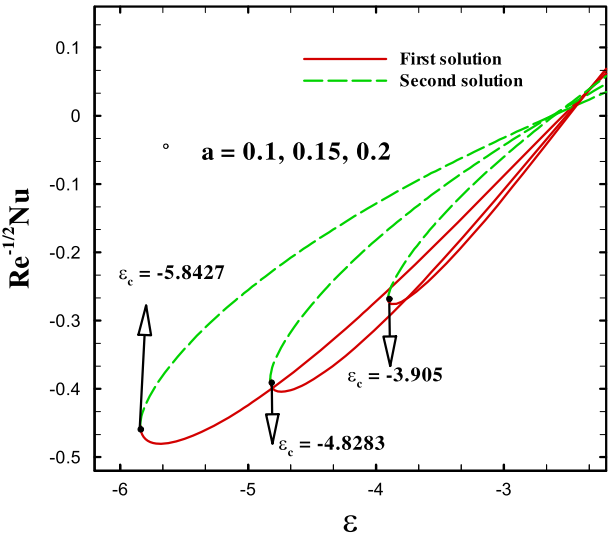

Fig. 21 Variation of $\mathrm{Re}^{-\frac{1}{2}}\mathrm{Nu}$ with ε for different values of a

3.1.4 Impact of numerous parameters on concentration profile

Figures 23, 24, 25, 26 and 27 enclose the behavior of reports on concentration gradient for various parameter considering two solutions. Further, graph evidently displays that rise in values of a, Nt declines concentration profile and it is faster in second solution when compared to first solution but opposite behavior can be observed for inclining values of Nb, Le and K. This is because the chemical reaction in this system causes the use of chemicals and therefore causes a reduction in the concentration gradient. The utmost vital result is that

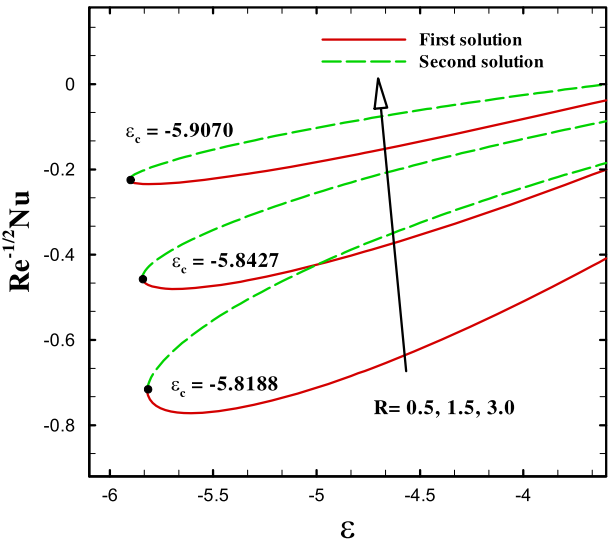

Fig. 22 Variation of $\mathrm{Re}^{-\frac{1}{2}}\mathrm{Nu}$ with ε for different values of a

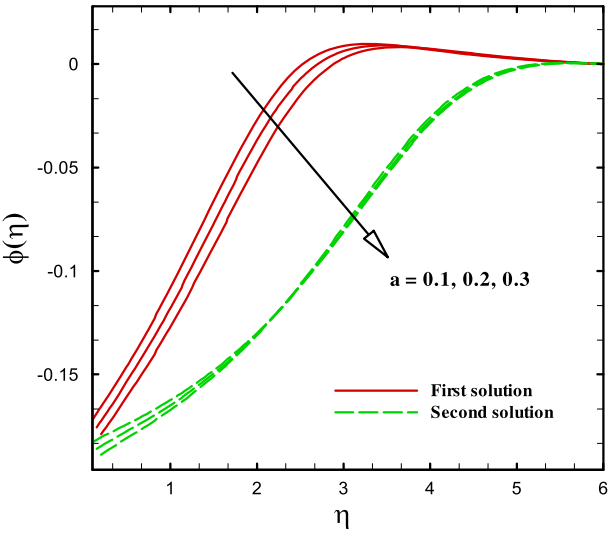

Fig. 23 $\phi(\eta)$ for several values of a

the chemical reaction of the first order has a tendency to diminish excessive exposure profiles in the solutal boundary layer.

4 Conclusions

In this article, a mathematical and cost-effective numerical simulation for a 2D stable, laminar and incompressible stream of magneto-Cross nanoliquid towards the region of moving thin

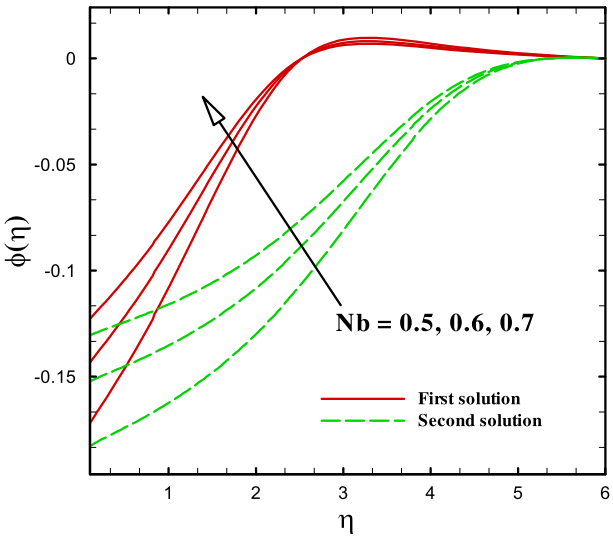

Fig. 24 $\phi(\eta)$ for several values of Nb

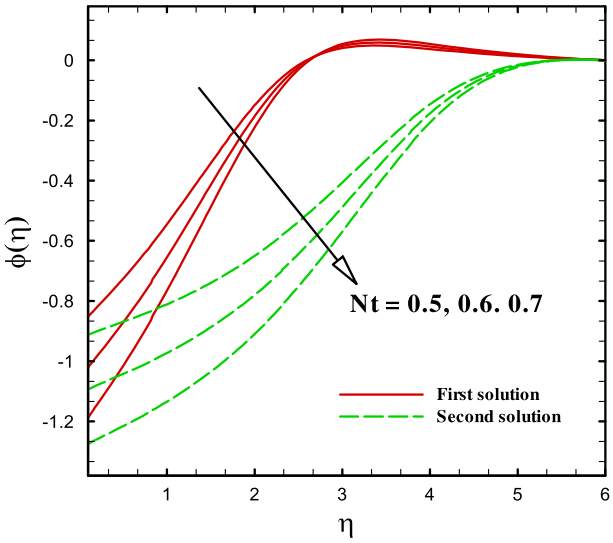

Fig. 25 $\phi(\eta)$ for several values of Nt

needle in the occurrence of Darcy–Forchheimer porous medium, mixed convection, Ohmic and viscous dissipation with chemical reaction is highlighted. The fluid model is unique in its way and has not been discussed in the literature yet. The reduced set of nonlinear ordinary differential equations were found using a numerical scheme that are reported and elaborated. The characteristics of velocity, thermal, concentration as well as skin friction, and Nusselt number have been deliberated under the influence of involved flow controlling physical parameters. The related outcomes to predictable degree include:

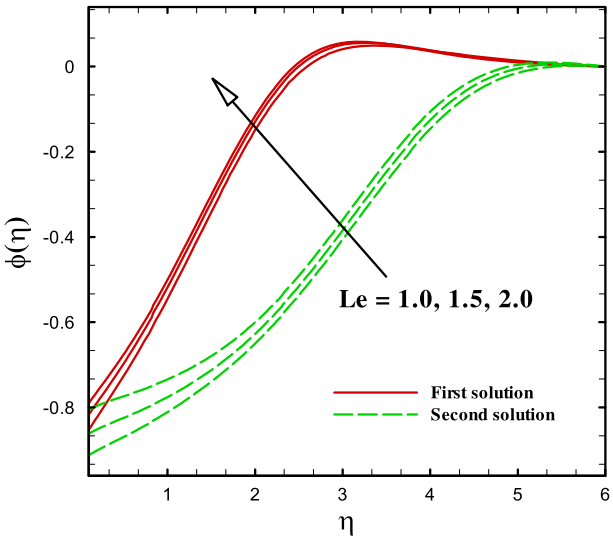

Fig. 26 $\phi(\eta)$ for several values of Le

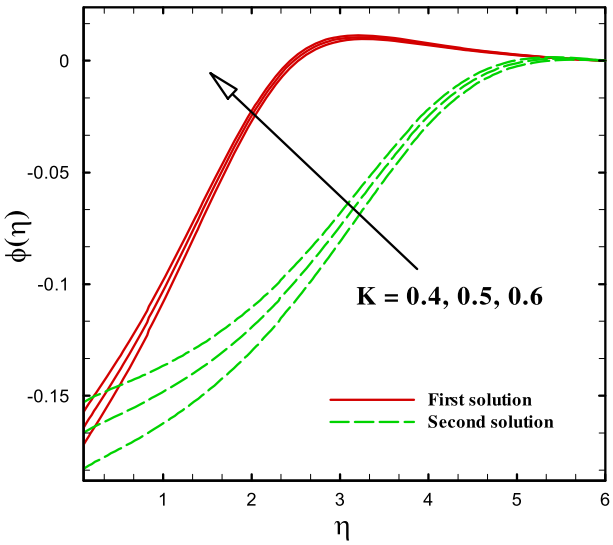

Fig. 27 $\phi(\eta)$ for several values of K

1. Advanced values of M, We and a slowdown the fluid velocity motion and thickness of its boundary layer associated with it.
2. Rise in values of a enhances the skin friction, but we detect opposite behavior for rise in values of M and We.
3. Upshot in thermophoresis parameter and Brownian motion parameter improves the thermal profile.
4. Rise in values of a improves the rate of heat transfer for diverse values of ε_c.

5. Upsurge in Lewis number and Brownian motion parameter enhances the concentration gradient, but opposite behavior is noticed for inclined values of thermophoresis parameter.

Funding The research was supported by the National Natural Science Foundation of China (Grant Nos. 11971142, 11871202, 61673169, 11701176, 11626101 and 11601485).

Declarations

Conflict of interest The authors declare that there is no conflict of interest.

References

1. J.L.S. Chen, T.N. Smith, Forced convection heat transfer from nonisothermal thin needles. ASME J. Heat Trans. **100**, 358–362 (1978)
2. A. Ishak, R. Nazar, I. Pop, Boundary layer flow over a continuously moving thin needle in a parallel free stream. Chin. Phys. Lett. **24**(10), 2895 (2007)
3. B. Souayeh, M.G. Reddy, P. Sreenivasulu, T. Poornima, M. Rahimi-Gorji, I.M. Alarifi, Comparative analysis on non-linear radiative heat transfer on MHD Casson nanofluid past a thin needle. J. Mol. Liq. **284**, 163–174 (2019)
4. M.K. Nayak, F. Mabood, O.D. Makinde, Heat transfer and buoyancy-driven convective MHD flow of nanofluids impinging over a thin needle moving in a parallel stream influenced by Prandtl number. Heat Transf. **49**(2), 655–672 (2020)
5. Y.-M. Chu, M.I. Khan, M.I. Ur Rehman, S. Kadry, M.K. Nayak, Flow and thermal management of MHD Cross nanofluids over a thin needle with auto catalysis chemical reactions. Int. J. Mod. Phys. B **34**(30), 2050287 (2020). https://doi.org/10.1142/S0217979220502872
6. S.U.S. Choi, Enhancing thermal conductivity of fluids with nanoparticles, Argonne National Lab., IL (United States), ANL/MSD/CP-84938; CONF-951135-29 (1995), https://www.osti.gov/biblio/196525. Accessed 03 Nov 2020
7. M.I. Khan, T. Hayat, M.I. Khan, A. Alsaedi, Activation energy impact in nonlinear radiative stagnation point flow of Cross nanofluid. Int. Commun. Heat Mass Transf. **91**, 216–224 (2018). https://doi.org/10.1016/j.icheatmasstransfer.2017.11.001
8. M. Azam, T. Xu, M. Khan, Numerical simulation for variable thermal properties and heat source/sink in flow of Cross nanofluid over a moving cylinder. Int. Commun. Heat Mass Transf. **118**, 104832 (2020). https://doi.org/10.1016/j.icheatmasstransfer.2020.104832
9. T. Hayat, M.I. Khan, M. Tamoor, M. Waqas, A. Alsaedi, Numerical simulation of heat transfer in MHD stagnation point flow of Cross fluid model towards a stretched surface. Results Phys. **7**, 1824–1827 (2017). https://doi.org/10.1016/j.rinp.2017.05.022
10. M. Ali, W.A. Khan, M. Irfan, F. Sultan, M. Shahzed, M. Khan, Computational analysis of entropy generation for cross-nanofluid flow. Appl. Nanosci. **10**(8), 3045–3055 (2020). https://doi.org/10.1007/s13204-019-01038-w
11. H. Darcy, in *Les Fontaines Publiques de la Ville de Dijon: Exposition et Application des Principes a Suivre et des Formulesa Employer dans les Questions de Distribution d'Eau*, ed. by V. Dalmont (Paris, 1856), p. 647
12. P. Forchheimer, Wasserbewegung durch boden. Z. Ver. Dtsch. Ing. **45**, 1782–1788 (1901)
13. M. Muskat, *The Flow of Homogeneous Fluids through Porous Media*, 1st edn. (J.W. Edwards Inc, Ann Arbor, MI, 1946)
14. M.I. Khan, F. Alzahrani, A. Hobiny, Z. Ali, Fully developed second order velocity slip Darcy-Forchheimer flow by a variable thicked surface of disk with entropy generation. Int. Commun. Heat Mass Transf. **117**, 104778 (2020). https://doi.org/10.1016/j.icheatmasstransfer.2020.104778
15. T. Hayat, F. Haider, A. Alsaedi, Darcy-Forchheimer flow with nonlinear mixed convection. Appl. Math. Mech. **41**(11), 1685–1696 (2020). https://doi.org/10.1007/s10483-020-2680-8
16. M.G. Reddy, P. Vijaya Kumari, G. Upender Reddy, K. Ganesh Kumar, B.C. Prasannakumara, A mathematical framework on Cattaneo–Christov model over an incessant moving needle. Multidiscip. Model. Mater. Struct. (2020). https://doi.org/10.1108/MMMS-01-2020-0012

17. N.S. Shashikumar, B.J. Gireesha, B. Mahanthesh, B.C. Prasannakumara, Brinkman-Forchheimer flow of SWCNT and MWCNT magneto-nanoliquids in a microchannel with multiple slips and Joule heating aspects. Multidiscip. Model. Mater. Struct. **14**(4), 769–786 (2018). https://doi.org/10.1108/MMMS-01-2018-0005
18. T. Hayat, F. Shah, A. Alsaedi, B. Ahmad, Entropy optimized dissipative flow of effective Prandtl number with melting heat transport and Joule heating. Int. Commun. Heat Mass Transf. **111**, 104454 (2020). https://doi.org/10.1016/j.icheatmasstransfer.2019.104454
19. M. Radhika, R.J.P. Gowda, R. Naveenkumar, Siddabasappa, B.C. Prasannakumara, Heat transfer in dusty fluid with suspended hybrid nanoparticles over a melting surface. Heat Transf. (2020). https://doi.org/10.1002/htj.21972
20. M. Ijaz, M. Ayub, M.Y. Malik, H. Khan, A.A. Alderremy, S. Aly, Entropy analysis in nonlinearly convective flow of the Sisko model in the presence of Joule heating and activation energy: the Buongiorno model. Phys. Scr. **95**(2), 025402 (2020). https://doi.org/10.1088/1402-4896/ab2dc7
21. M.I. Khan, Transportation of hybrid nanoparticles in forced convective Darcy-Forchheimer flow by a rotating disk. Int. Commun. Heat Mass Transf. **122**, 105177 (2021)
22. M. Ijaz Khan, F. Haq, S.A. Khan, T. Hayat, M. Imran Khan, Development of thixotropic nanomaterial in fluid flow with gyrotactic microorganisms, activation energy, mixed convection. Comput. Methods Progr. Biomed. **187**, 105186 (2020). https://doi.org/10.1016/j.cmpb.2019.105186
23. M.I. Khan, F. Alzahrani, Nonlinear dissipative slip flow of Jeffrey nanomaterial towards a curved surface with entropy generation and activation energy. Math. Comput. Simul. **185**, 47–61 (2021)
24. M.I. Khan, F. Alzahrani, Free convection and radiation effects in nanofluid (silicon dioxide and molybdenum disulfide) with second order velocity slip, entropy generation, Darcy-Forchheimer porous medium. Int. J. Hydrog. Energy **46**, 1362–1369 (2021)
25. F. Garoosi, G. Bagheri, M.M. Rashidi, Two phase simulation of natural convection and mixed convection of the nanofluid in a square cavity. Powder Technol. **275**, 239–256 (2015). https://doi.org/10.1016/j.powtec.2015.02.013
26. M. Bhattacharya, T. Basak, H.F. Oztop, Y. Varol, Mixed convection and role of multiple solutions in lid-driven trapezoidal enclosures. Int. J. Heat Mass Transf. **63**, 366–388 (2013). https://doi.org/10.1016/j.ijheatmasstransfer.2013.03.028
27. M.I. Khan, F. Alzahrani, Cattaneo-Christov Double Diffusion (CCDD) and magnetized stagnation point flow of non-Newtonian fluid with internal resistance of particles. Phys. Scr. **95**, 125002 (2020)
28. N.S. Anuar, N. Bachok, N.M. Arifin, H. Rosali, Role of multiple solutions in flow of nanofluids with carbon nanotubes over a vertical permeable moving plate. Alex. Eng. J. **59**(2), 763–773 (2020). https://doi.org/10.1016/j.aej.2020.02.015
29. Y. Gupta, P. Rana, O.A. Beg, A. Kadir, Multiple solutions for slip effects on dissipative magneto-nanofluid Transport phenomena in porous media: stability analysis. J. Appl. Comput. Mech. **6**(4), 956–967 (2020). https://doi.org/10.22055/jacm.2019.30144.1689
30. I. Mustafa, Z. Abbas, A. Arif, T. Javed, A. Ghaffari, Stability analysis for multiple solutions of boundary layer flow towards a shrinking sheet: analytical solution by using least square method. Phys. Stat. Mech. Appl. **540**, 123028 (2020). https://doi.org/10.1016/j.physa.2019.123028